

# Rockfall from an increasingly unstable mountain slope driven by climate warming

Received: 18 May 2023

Accepted: 30 January 2024

Published online: 23 February 2024

 Check for updates

Markus Stoffel <sup>1,2,3</sup>✉, Daniel G. Trappmann<sup>1,4</sup>, Mattias I. Coullie<sup>1</sup>,  
Juan A. Ballesteros Cánovas <sup>1,2,5</sup> & Christophe Corona <sup>1,6</sup>

Rockfall in high-mountain regions is thought to be changing due to accelerating climate warming and permafrost degradation, possibly resulting in enhanced activity and larger volumes involved in individual falls. Yet the systematic lack of long-term observations of rockfall largely hampers an in-depth assessment of how activity may have been altered by a warming climate. Here we compile a continuous time series from 1920 to 2020 of periglacial rockfall activity using growth-ring records from 375 trees damaged by past rockfall at Täschgufer (Swiss Alps). We show that the ongoing warming favours the release of rockfall and that changes in activity correlate significantly with summer air temperatures at interannual and decadal timescales. An initial increase in rockfall occurred in the late 1940s to early 1950s following early twentieth century warming. From the mid-1980s, activity reached new and hitherto unprecedented levels. This long-term record of rockfall activity can help to inform the design of vital mitigation and risk reduction measures in inhabited mountain environments.

Rockfall is among the processes that receive most attention in alpine areas by the general public due to its presumed intimate relation with permafrost<sup>1–3</sup>, which is found to be degrading widely in high-mountain environments<sup>4,5</sup>. Heatwaves in the Alps during 2003, 2015 and 2022 caused spikes in rockfall incidents<sup>6</sup>, raising concerns about their destabilizing effects on slopes<sup>7,8</sup>. Further climate warming and permafrost degradation are expected to worsen slope stability, endangering mountain communities and transportation routes<sup>9</sup>.

Rockfall can involve various volumes, from individual boulders to rock avalanches<sup>10</sup>. Here we use the term to describe individual events consisting of single boulders or small rock masses (mostly <10 m<sup>3</sup>) released from a cliff or a steep slope to proceed downslope by free fall, bouncing along ballistic trajectories or rolling on talus slopes<sup>11</sup>. Most rockfall is triggered from bedrock along new or previously existing discontinuities<sup>12</sup> by seismic shaking, snowmelt dynamics, precipitation, permafrost degradation or freeze–thaw conditions<sup>13</sup>. The complex nature of rockfall triggers makes it challenging to identify climate-related drivers.

Several authors suggest recent heatwaves have increased rockfall in the Alps, especially in areas with degrading permafrost<sup>2,3,14</sup>. Field evidence supports the assumption of enhanced permafrost degradation favouring the occurrence of rockfall<sup>15,16</sup>. However, the relationship between climate change, permafrost degradation and rockfall remains poorly understood due to limited long-term high-elevation climate data, the complexity of mountain terrain and the scarcity of systematic, multi-decadal rockfall records<sup>1,16,17</sup>. The difficulty lies, in part, in the paucity of high-elevation weather records and the limited performance of climate models in complex mountain terrain<sup>18,19</sup> and also in the complex, or indirect, relation between slope instability and climate<sup>7</sup>. In addition, existing rockfall datasets tend to suffer from non-uniform observation rates<sup>20</sup> and biases towards recent and larger rockfalls that caused damage to infrastructure<sup>21</sup>.

All these uncertainties have hitherto hindered efforts to quantify trends and model climate impacts in the cryosphere<sup>4</sup>. Here we examine the link between climate warming and annual rockfall rates over the

<sup>1</sup>Climate Change Impacts and Risks in the Anthropocene (C-CIA), Institute for Environmental Sciences, University of Geneva, Geneva, Switzerland.

<sup>2</sup>dendrolab.ch, Department of Earth Sciences, University of Geneva, Geneva, Switzerland. <sup>3</sup>Department F.-A. Forel for Environmental and Aquatic Sciences, University of Geneva, Geneva, Switzerland. <sup>4</sup>Bayerische Staatsforsten, Martin bei Lofer, Germany. <sup>5</sup>National Museum of Natural Sciences, MNCN-CSIC, Madrid, Spain. <sup>6</sup>Université Grenoble Alpes, CNRS LECA, Grenoble, France. ✉e-mail: [Markus.Stoffel@unige.ch](mailto:Markus.Stoffel@unige.ch)

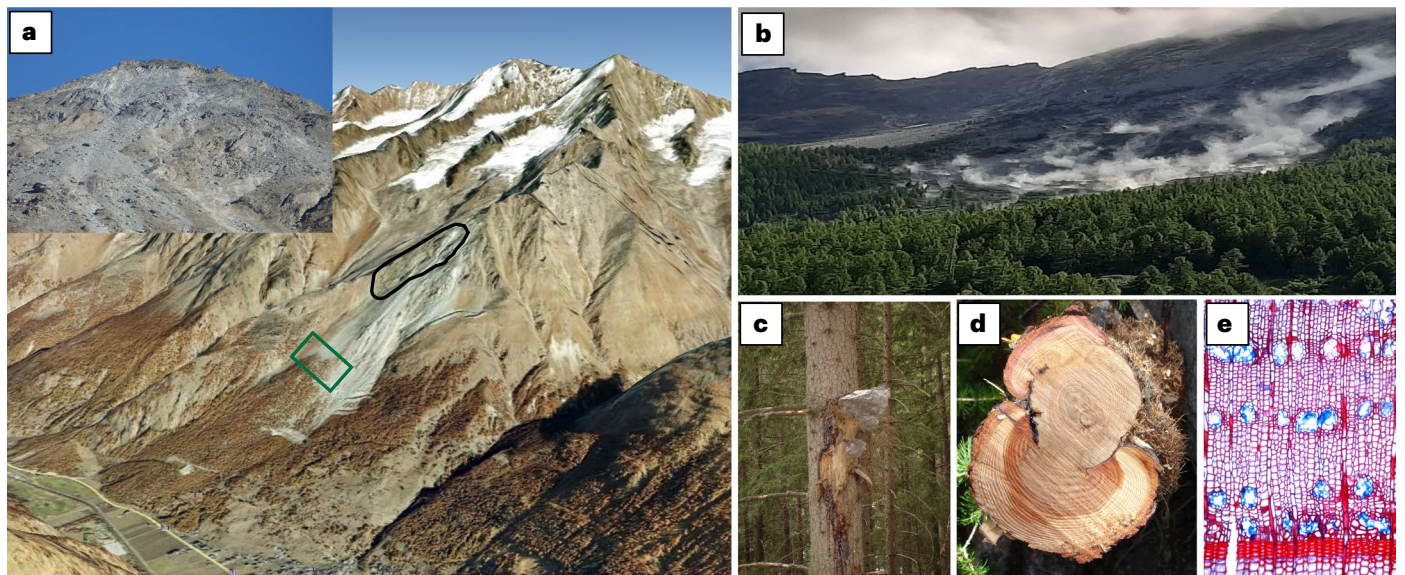


**Fig. 1** Rockfall activity from a slope affected by thawing permafrost can be recorded in trees growing at the forest fringe. **a**, Rockfall at Täschgufer (Swiss Alps) originates from heavily disintegrated, gneissic outcrops (inset) situated in permafrost-dominated environments between 2,900 and 2,450 m asl (black shape). Forest fringe is designated by the green shape. **b, c**, Dust clouds generated by a larger rockfall at an adjacent site on 8 June 2019 (**b**) and the subsequent

impact on a tree (**c**). **d, e**, European larch (*Larix decidua* Mill.) trees can overgrow rockfall injuries (**d**) by forming chaotic callus tissue and tangential rows of traumatic resin ducts (**e**). These anatomical markers are utilized to date past rockfall with sub-seasonal precision. Credit: **a**, GoogleEarth, Landsat/Copernicus (main photo); Markus Stoffel (inset).

past 100 years and suggest that permafrost degradation has indeed increased rockfall at a site in the Swiss Alps.

### Seasonal changes in rockfall activity

We reconstruct a century (1920–2020) of rockfall activity by dendrogeomorphic techniques to date rockfall damage inflicted on European larch (*Larix decidua* Mill.) trees<sup>22</sup>. The study site, Täschgufer (Swiss Alps, 46° 4' N, 7° 47' E; Fig. 1a), experiences frequent rockfall from heavily disintegrated gneissic outcrops<sup>23</sup> striking SSW and dipping WNW with angles of 40–80°. The main source areas of rockfall (2,450–2,900 m above sea level (asl)) are at the limit between seasonal frost and permafrost environments; the presence of permafrost has been confirmed locally<sup>24</sup>.

We sampled 375 *L. decidua* trees along a 177-m-wide transect at the forest fringe where trees intercept rockfall. Trees at the site are hit by rocks with median and mean volumes of 0.74 and 1.39 m<sup>3</sup> (values based on 87 recent deposits). Smaller rock fragments are typically deposited upslope in the transit zone due to its substantial length (1,290 m) and the difference in elevation (770 m) between the source areas and the forest fringe (Fig. 1b).

Rockfall damages trees by causing injuries (Fig. 1c) that the tree will attempt to heal with chaotic callus tissue (Fig. 1d) and the formation of tangential rows of traumatic resin ducts (TRDs) within 7–10 days after an impact to protect the wood from pathogens<sup>25</sup>. These injuries and TRDs serve as reliable indicators for dating past rockfall<sup>22</sup>. If wounding occurred during the growing season (which lasts from mid-May to late September at the study site<sup>26</sup>), past rockfall can be dated at sub-seasonal resolution<sup>22</sup> (Methods).

Our analysis revealed 1,450 growth disturbances (GDs; that is, injuries and TRDs) caused by rockfall between 1835 and 2020. With a mean age of sampled *L. decidua* trees of 66 ± 37 years, we limit interpretation of findings to the last 100 years (1920–2020) for which we have ≥88 trees and 1,357 GDs; of these, 408 GDs are dated with sub-seasonal precision.

On the basis of a Monte Carlo modelling approach of the intra-ring position of GDs, a shift in the seasonal occurrence of rockfall is observed (Fig. 2): between 1920 and 1969, almost all injuries (91%;  $n = 10$ ) and a

majority of GD (55%;  $n = 29$ ) occurred during dormancy (1 October–15 May; Fig. 2a). However, after 1970, the relative frequency of winter–spring rockfall decreased, with a noticeable increase in ‘warm-season’ rockfall (16 May–30 September; 51% of all injuries;  $n = 37$ ; 37% of all GDs;  $n = 130$ ). Whereas only 9% ( $n = 1$ ) and 45% ( $n = 24$ ) of all rockfall occurred in summer and early fall (that is, 16 May–30 September) before 1969, ‘warm-season’ activity has risen sharply to account for 49% ( $n = 35$ ) and 63% ( $n = 225$ ) after 1970 and even to 58% ( $n = 18$ ) and 70% ( $n = 42$ ) since 2010. Local polynomial regressions fitted to Monte Carlo modelled days of rockfall occurrence (Fig. 2a) confirm this shift, which, according to quantile-based regression slopes and the Theil–Sen estimator (Methods), accounts for 63–67 days for injuries and 42–43 days for GDs over the past century (Fig. 2b, c). This marked change in rockfall seasonality from dormancy (D) to early (EE) and mid-early wood (ME)—that is, mid-May to late June—aligns with direct observations at the site and the occurrence of recent rockfall events in June (Fig. 1b); this shift can probably be ascribed to a shift from seasonal, near-surface freeze–thaw activity in winter and spring to recent and more enhanced permafrost instability at greater depths.

### Accelerating climate warming propels rockfall activity

Mean annual rockfall impact counts show a sharp increase—from 4.76 (1920–1940) to 31.23 (1990–2011)—over time. This increase is probably influenced by the growing number (from 88 to 375) and increasing size (from 7.98 to 87.19 m when summing all tree diameters at breast height, or DBH) of trees and their distribution across the slope by 2011. We sampled 123 trees in 2021 to extend the record and obtain a mean annual rockfall count of seven (2012–2020) and a DBH sum of 20.32 m. To remove biases related to changing sample depth and target size, we calculated conditional impact probabilities (CIPs) to quantify the range of the slope covered by trees in any given year and to derive the likelihood of a rockfall passing the slope without impacting any sampled tree or—on the contrary—hitting multiple trees on its trajectory<sup>27,28</sup>. The CIP takes account of both forest (that is, stand density, tree position, tree diameter, forest stand structure) and rockfall (clast diameter) characteristics to yield realistic annual estimates (Methods) of past rockfall activity<sup>27</sup>.

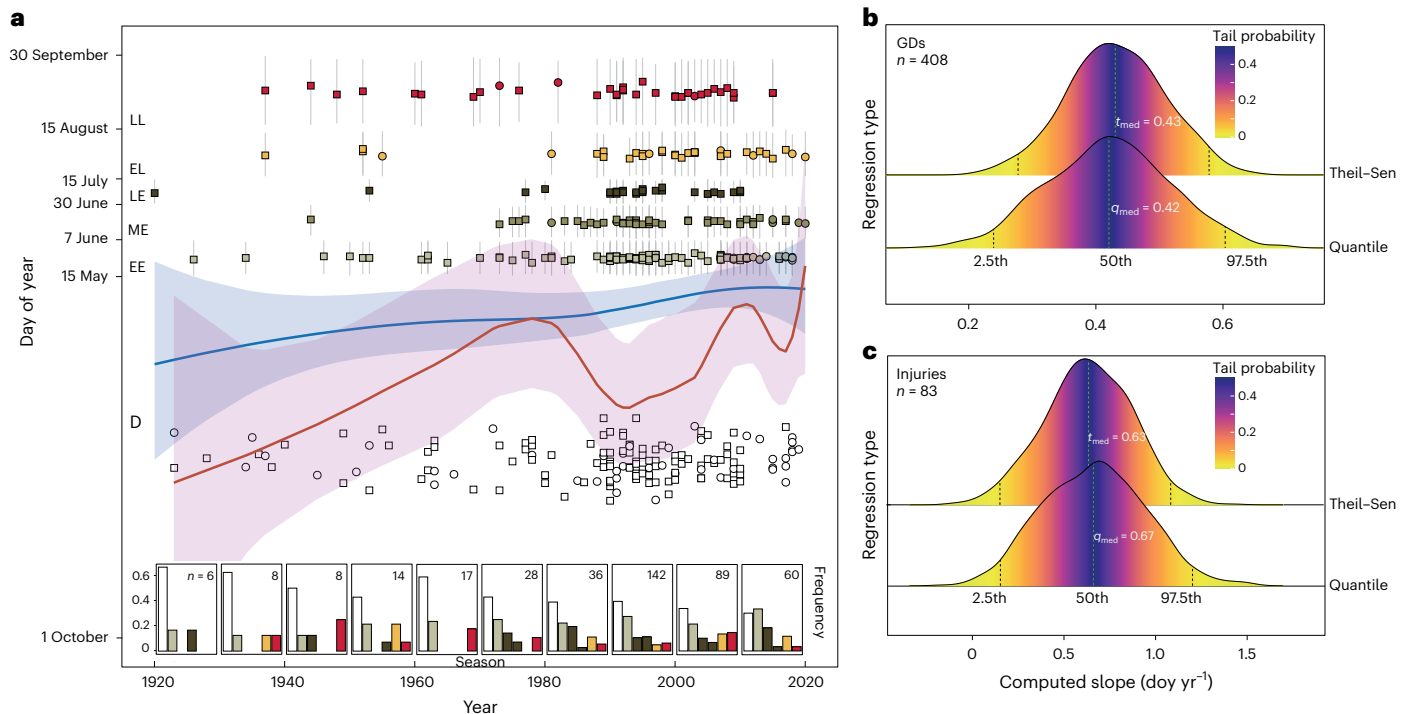


**Fig. 2 | Shifts in rockfall seasonality over time, with activity occurring progressively later in the year. a**, Sub-seasonal frequency of occurrence (inset) and Monte Carlo (MC) modelled day of year (doy) of rockfall from 1920 to 2020. The MC approach models a box plot for the seasonal occurrence of each injury (circles) and GD (rectangles), thereby considering uncertainties in actual rockfall dates. Local polynomial regressions are shown with blue (injuries;  $n = 83$ ) and red

(GD;  $n = 408$ ) lines and 95% confidence intervals. **b, c**, Tail probabilities for annual shifts in rockfall seasonality for GDs (**b**) and injuries (**c**) only. Damage in trees is given as D = dormancy (white); EE = early early wood (light grey); ME = mid-early wood (grey); LE = late early wood (dark grey); EL = early latewood (yellow) and LL = late latewood (red).

We find substantial increases in rockfall frequency from the late 1940s to the early 1950s and especially since the mid-1980s. At the inter-annual scale, rockfall frequency exhibits significant correlation with air temperatures, with highest values recorded for a time window comprised between 13 July and 26 August ( $r = 0.48$ ,  $p < 0.01$ ; Fig. 3a). This correlation remains significant ( $r = 0.37$ ;  $p < 0.01$ ) after detrending of both datasets to account for the accelerating warming and increased rockfall activity.

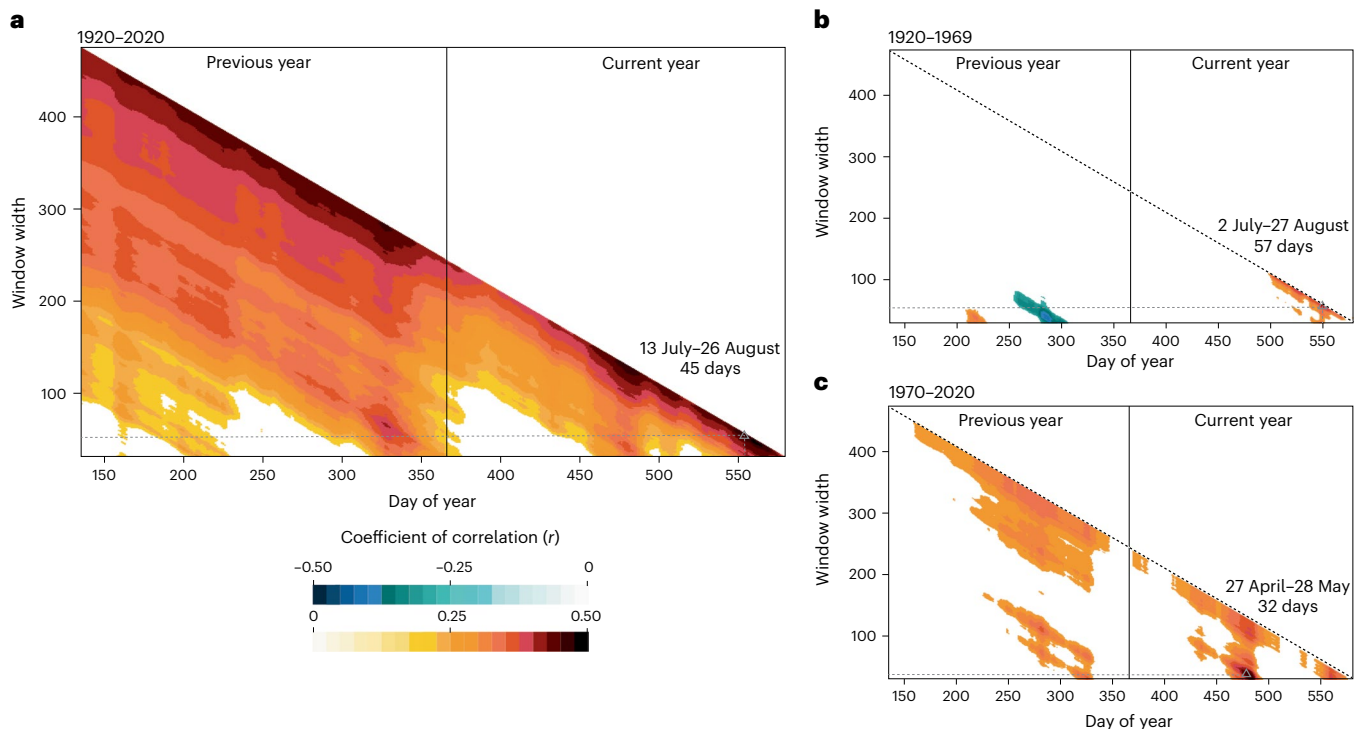
Significant correlations were limited mostly to summer air temperatures between 1920 and 1969 (2 July–27 August;  $r = 0.41$ / $r = 0.40$  ( $p < 0.01$ ) before/after detrending; Fig. 3b). Since 1970, however, we find significant correlations for both late spring (27 April–28 May;  $r = 0.47$ / $r = 0.47$ ,  $p < 0.01$ ) and for a short summer window (14 July–16 August;  $r = 0.39$ / $r = 0.37$ ,  $p < 0.01$ ; Fig. 3c). These findings are confirmed by eyewitness observations regarding changes in rockfall seasonality at the site. By contrast, precipitation does not correlate with rockfall activity (Supplementary Fig. 1).

Figure 4 illustrates annual variations of rockfall rates and correlations with air temperatures and temperature and rockfall data smoothed with a nine-year spline to retrieve decadal fluctuations in process activity. Despite the loss of degrees of freedom inherent to smoothing, correlations remain significant ( $r = 0.69$ ;  $p < 0.01$ ), pointing to the assumed key role of warm summers (13 July–26 August) and their contribution to permafrost degradation<sup>29,30</sup> in driving rockfall<sup>3</sup>. Agreement between summer air temperatures and rockfall occurrence is noted between the late 1940s and early 1950s. This time window marks the end of the ‘Early Twentieth Century Warming’ (ETCW)<sup>31</sup>, the most prominent accelerated warming phase before current warming, when temperature change was outside internal variability<sup>32</sup>. From the mid-1950s to the mid-1980s, an episode characterized by cooler conditions resulted in fewer rockfalls at the site. With the onset of accelerating climate warming in the mid-1980s, rockfall activity is again increasing. Eyewitness reports and expert opinions

confirm the reconstructed increase in rockfall, which resulted in damage to infrastructure in the valley floor and led to the construction of rockfall dams south of the study site in 1988, 1989, 1996, 1997 and 1998<sup>23</sup> (Fig. 1a).

Although we can provide evidence for a correlation between warming summer air temperatures and rockfall rates, results also point to some delay—or a lag<sup>33</sup>—between the driver and actual trigger of rockfall. Figures 3a and 4 show that enhanced rockfall occurs when consecutive warm summers are recorded, probably favouring instability through the melting and destabilization of frozen ground at larger-than-normal depths<sup>34</sup>. After several very warm summers recorded in the Alps between 1943 and 1946 and a heatwave in 1947<sup>35</sup>, we observe a sustained, multi-year increase in rockfall activity from 1949 to 1953. Likewise, the sharp rise in summer temperatures since the 1980s<sup>18,36</sup>—and particularly between 1990 and 1993—resulted in enhanced rockfall peaking in 1994 and 1995 (Fig. 4 and Extended Data Figs. 1–3). Rockfall has remained substantial since the mid-1990s and its incidence tends to follow the summer air temperature evolution.

Whereas decadal trends show a strong correlation between warming summer air temperatures and increased rockfall activity, this connection becomes less apparent at shorter, interannual timescales. This is because snow cover, ground heat transport, frost weathering or mechanical processes<sup>37–40</sup> play a critical role in driving inter-annual rockfall activity, alongside potential lag effects discussed earlier. One can hypothesize that early and rapid snowmelt in late spring can intensify active-layer thawing<sup>41</sup> and ice erosion in fractures<sup>29</sup>, leading to decreased shear resistance and increased shear forces due to higher hydrostatic pressure from meltwater in clefts<sup>38</sup>. This, in turn, results in greater instability during early summer. In the absence of local data on ground heat or active-layer thawing, we can only compare the rockfall reconstruction with borehole temperature data from Corvatsch in the Swiss Alps<sup>42</sup> (Supplementary Fig. 2). This comparison reveals significant



**Fig. 3 | Warming air temperatures correlate with interannual fluctuations in rockfall, with recent activity associated predominantly with warm spring temperatures.** Interannual correlations between rockfall and air temperatures were assessed across various time windows starting on 15 May of the year preceding tree damage and ending on 30 September of the year in which damage occurred. **a**, From 1920 to 2020, warm temperatures positively influence rockfall across a range of shorter (30 days) to longer (450 days) time windows, with highest correlations observed for 13 July–26 August (45 days;  $r = 0.48$ ,  $p < 0.01$ ). In addition, the significant correlations found from early June (around day of

year 160) to early December (340) in the year preceding rockfall and window widths of 280 to 450 days point to some delay—or a lag—between the driver and actual trigger of rockfall. The hat enhanced rockfall occurs when consecutive warm summers are recorded, probably favouring instability through the melting and destabilization of frozen ground at larger-than-normal depths. **b**, Between 1920 and 1969, the highest correlation extends from 2 July–27 August (57 days;  $r = 0.41$ ,  $p < 0.01$ ). **c**, After 1970, rockfall activity correlates best with warm air temperatures in spring (27 April–28 May; 32 days;  $r = 0.47$ ,  $p < 0.01$ ) and to a lesser degree to summer warmth (14 July–16 August; 33 days;  $r = 0.39$ ,  $p < 0.01$ ).

agreement between early summer (27 May–25 June) borehole temperatures and rockfall at Täschgufer ( $r = 0.69$ ;  $p < 0.01$ ; 2001–2020).

Before the actual occurrence of rockfall, frost weathering plays a crucial role in gradually weakening rock strength and creating conditions for instability in newly exposed bedrock<sup>43</sup>. Therefore, we hypothesize that following massive rockfall activity at the site in the late 1980s and 1990s, much of the heavily weathered material was eroded, and newly exposed bedrock now needs to be weakened to become available for future rockfall<sup>44,45</sup>.

### A benchmark site for rockfall

Rockfall is a prominent geomorphic process in steep bedrock landscapes, but monitoring and detecting changes in its activity are challenging due to the lack of long-term records<sup>46,47</sup>. In this study, a systematic century-long (1920–2020) time series of rockfall was reconstructed from a degrading permafrost slope. Unlike previous work, focusing on larger failures ( $10^3$ – $10^6$  m<sup>3</sup>), we investigated rockfall involving individual boulders and volumes of individual events  $<10$  m<sup>3</sup>. The latter are more frequent and directly responsive to climate variability and change<sup>48</sup> and often represent a more imminent threat to mountain communities<sup>48,49</sup>.

Interannual and decadal trends show correlations between rockfall activity and summer air temperatures, with warmer temperatures associated with more rockfall. Enhanced activity during the ETCW and since the mid-1980s therefore align with the understanding that degrading permafrost contributes to slope instability and rockfall<sup>36</sup>. However, interannual fluctuations are also influenced by factors such as snow cover, ground heat and soil moisture<sup>37–40</sup> for which data is still critically lacking in mountain environments. Similar agreement between enhanced rockfall and air temperature was observed at a

nearby site in the Swiss Alps with a comparable record of past rockfall activity (Supplementary Fig. 3), suggesting a broader influence of climate warming and permafrost degradation on rockfall.

The rockfall record provided here, along with the influence of summer air temperatures on rockfall activity, has regional significance due to its length, the substantial amount of data collected and the valuable insights it offers into the seasonality of rockfall. Although we cannot draw conclusions on how rockfall activity evolves in other high-mountain regions, the Täschgufer site can serve as a benchmark site for future research, as its long time series represents a crucial step in comprehensively documenting changes in rockfall activity in similar locations.

Warming air temperatures in the European Alps<sup>50</sup>, particularly at high elevations dominated by the cryosphere<sup>5</sup>, are now clearly outpacing global averages. Accelerated climate warming and mountain permafrost degradation are expected to lead to increased rockfall in the Alps. However, we show that the response of a rockfall system may not be linear but involve lags and system-specific controls. In a broader context, however, continued warming is expected to promote increased rockfall activity from steep permafrost areas, which, in turn, will necessitate adjustments in increasingly unstable mountain slopes. These changes are likely to have significant repercussions on the physical, biological and human systems in mountain environments<sup>4</sup>.

### Online content

Any methods, additional references, Nature Portfolio reporting summaries, source data, extended data, supplementary information, acknowledgements, peer review information; details of author contributions and competing interests; and statements of data and code availability are available at <https://doi.org/10.1038/s41561-024-01390-9>.

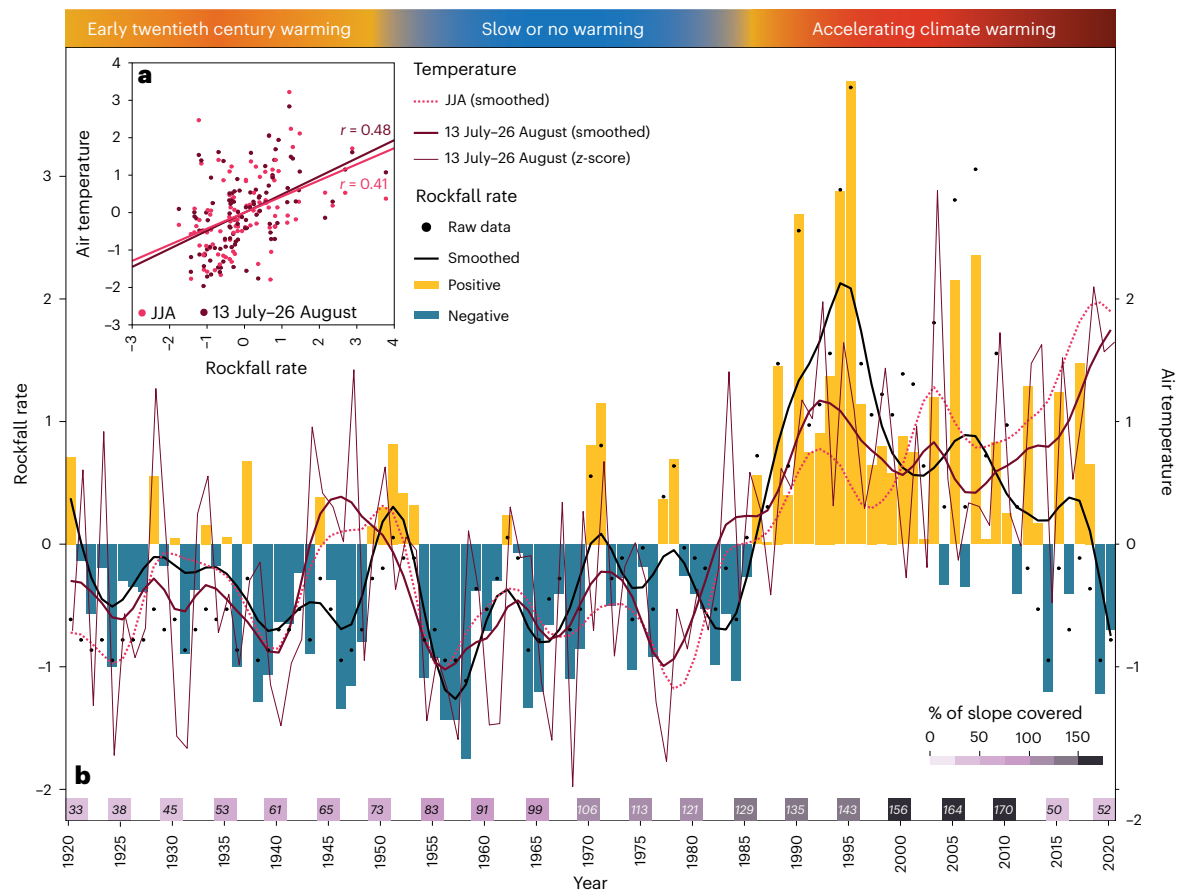


**Fig. 4 | Rockfall rates at Täschgufer closely follow summer air temperatures, especially if warmer conditions persist over several summers.** Evolution of raw (black dots) and bias-corrected (blue and yellow) annual rockfall activity and nine-year spline-smoothed rockfall trends (black curve) at Täschgufer between 1920 and 2020. Both temperatures and rockfall rates are plotted as deviations (z-scores) from their 1920–2020 means. The thin (annual) and bold (spline smoothed) purple curves show z-score data for 13 July–26 August (Fig. 3); the red dotted curve shows smoothed June–August (JJA) air temperatures at the site. The

latter correlation remains significant at decadal timescales with  $r = 0.69$  ( $p < 0.01$ ). Rockfall activity first increased in the late 1940s and early 1950s to peak massively after the mid-1980s. **a**, Rockfall correlates with annual JJA ( $r = 0.41$  ( $p < 0.01$ )) and 13 July–26 August ( $r = 0.48$  ( $p < 0.01$ )) air temperatures. **b**, The combination of DBH with the mean impact circles (defined by the mean diameter of rockfall fragments) yields an estimate of the percentage of the slope for which rockfall will be intercepted by trees in any given year or decade and therefore allows definition of periods for which activity is either over- (>100%) or underestimated (<100%).

## References

- Ravel, L. & Deline, P. Climate influence on rockfalls in high-Alpine steep rockwalls: the north side of the Aiguilles de Chamonix (Mont Blanc massif) since the end of the ‘Little Ice Age’. *Holocene* **21**, 357–365 (2011).
- Chiarle, M., Geertsema, M., Mortara, G. & Clague, J. J. Relations between climate change and mass movement: perspectives from the Canadian Cordillera and the European Alps. *Glob. Planet. Change* **202**, 103499 (2021).
- Ravel, L., Magnin, F. & Deline, P. Impacts of the 2003 and 2015 summer heatwaves on permafrost-affected rock-walls in the Mont Blanc massif. *Sci. Total Environ.* **609**, 132–143 (2017).
- Hock, R. et al. in *IPCC Special Report on the Ocean and Cryosphere in a Changing Climate* (eds. Pörtner et al.) <https://doi.org/10.1017/9781009157964.004> (Cambridge Univ. Press, 2019).
- Biskaborn, B. K. et al. Permafrost is warming at a global scale. *Nat. Commun.* **10**, 264 (2019).
- Schiermeier, Q. Alpine thaw breaks ice over permafrost’s role. *Nature* **424**, 712–712 (2003).
- Stoffel, M. & Huggel, C. Effects of climate change on mass movements in mountain environments. *Prog. Phys. Geogr.* **36**, 421–439 (2012).
- Paranunzio, R., Laio, F., Chiarle, M., Nigrelli, G. & Guzzetti, F. Climate anomalies associated with the occurrence of rockfalls at high-elevation in the Italian Alps. *Nat. Hazards Earth Syst. Sci.* **16**, 2085–2106 (2016).
- Coe, J. A. Bellwether sites for evaluating changes in landslide frequency and magnitude in cryospheric mountainous terrain: a call for systematic, long-term observations to decipher the impact of climate change. *Landslides* **17**, 2483–2501 (2020).
- Dikau, R., Brunsden, D., Shrott, L. & Ibsen, M. *Landslide Recognition: Identification, Movement and Causes* (Wiley, 1996).
- Evans, S. G. & Hungr, O. The assessment of rockfall hazard at the base of talus slopes. *Can. Geotech. J.* **30**, 620–636 (1993).
- Selby, M. J. *Hillslope Materials and Processes* (Oxford Univ. Press, 1993).
- Collins, B. D. & Stock, G. M. Rockfall triggering by cyclic thermal stressing of exfoliation fractures. *Nat. Geosci.* **9**, 395–400 (2016).
- Fischer, L., Purves, R. S., Huggel, C., Noetzi, J. & Haeberli, W. On the influence of topographic, geological and cryospheric factors on rock avalanches and rockfalls in high-mountain areas. *Nat. Hazards Earth Syst. Sci.* **12**, 241–254 (2012).
- Krautblatter, M., Funk, D. & Günzel, F. K. Why permafrost rocks become unstable: a rock-ice-mechanical model in time and space. *Earth Surf. Process. Landf.* **38**, 876–887 (2013).

16. Luethi, R., Gruber, S. & Ravel, L. Modelling transient ground surface temperatures of past rockfall events: towards a better understanding of failure mechanisms in changing periglacial environments. *Geogr. Ann. Ser. A Phys. Geogr.* **97**, 753–767 (2015).
17. Huggel, C., Clague, J. J. & Korup, O. Is climate change responsible for changing landslide activity in high mountains? *Earth Surf. Process. Landf.* **37**, 77–91 (2012).
18. Gobiet, A. et al. 21st century climate change in the European Alps—a review. *Sci. Total Environ.* **493**, 1138–1151 (2014).
19. Pepin, N. C. et al. Climate changes and their elevational patterns in the mountains of the world. *Rev. Geophys.* **60**, e2020RG000730 (2022).
20. Mourey, J. et al. Multi-method monitoring of rockfall activity along the classic route up Mont Blanc (4809 m a.s.l.) to encourage adaptation by mountaineers. *Nat. Hazards Earth Syst. Sci.* **22**, 445–460 (2022).
21. Guerin, A. et al. Quantifying 40 years of rockfall activity in Yosemite Valley with historical structure-from-motion photogrammetry and terrestrial laser scanning. *Geomorphology* **356**, 107069 (2020).
22. Stoffel, M. & Corona, C. Dendroecological dating of geomorphic disturbance in trees. *Tree-Ring Res.* **70**, 3–20 (2014).
23. Stoffel, M. et al. Analyzing rockfall activity (1600–2002) in a protection forest—a case study using dendrogeomorphology. *Geomorphology* **68**, 224–241 (2005).
24. Gruber, S. & Hoelzle, M. Statistical modelling of mountain permafrost distribution: local calibration and incorporation of remotely sensed data. *Permafrost Periglacial Processes* **12**, 69–77 (2001).
25. Nagy, N. E., Franceschi, V. R., Solheim, H., Krekling, T. & Christiansen, E. Wound-induced traumatic resin duct development in stems of Norway spruce (Pinaceae): anatomy and cytochemical traits. *Am. J. Bot.* **87**, 302–313 (2000).
26. Stoffel, M., Lièvre, I. & Monbaron, M. Seasonal timing of rockfall activity on a forested slope at Täschgüfer (Swiss Alps)—a dendrochronological approach. *Z. Geomorphol.* **49**, 89–106 (2005).
27. Trappmann, D., Corona, C. & Stoffel, M. Rolling stones and tree rings: a state of research on dendrogeomorphic reconstructions of rockfall. *Prog. Phys. Geogr.* **37**, 701–716 (2013).
28. Mainieri, R. et al. Dating of rockfall damage in trees yields insights into meteorological triggers of process activity in the French Alps. *Earth Surf. Process. Landf.* **45**, 2235–2250 (2020).
29. Hasler, A., Gruber, S. & Beutel, J. Kinematics of steep bedrock permafrost. *J. Geophys. Res. Earth Surf.* **117**, F01016 (2012).
30. Davies, M. C. R., Hamza, O. & Harris, C. The effect of rise in mean annual temperature on the stability of rock slopes containing ice-filled discontinuities. *Permafrost Periglacial Processes* **12**, 137–144 (2001).
31. Hegerl, G. C., Brönnimann, S., Schurer, A. & Cowan, T. The early 20th century warming: anomalies, causes, and consequences. *WIREs Clim. Change* **9**, e522 (2018).
32. Hegerl, G. C. et al. Multi-fingerprint detection and attribution analysis of greenhouse gas, greenhouse gas-plus-aerosol and solar forced climate change. *Clim. Dyn.* **13**, 613–634 (1997).
33. Crozier, M. J. Deciphering the effect of climate change on landslide activity: a review. *Geomorphology* **124**, 260–267 (2010).
34. Noetzi, J. & Gruber, S. Transient thermal effects in Alpine permafrost. *Cryosphere* **3**, 85–99 (2009).
35. Schär, C. et al. The role of increasing temperature variability in European summer heatwaves. *Nature* **427**, 332–336 (2004).
36. IPCC *Climate Change 2021: The Physical Science Basis* (eds Masson-Delmotte, V. et al.) (Cambridge Univ. Press, 2021).
37. Gubler, S., Endrizzi, S., Gruber, S. & Purves, R. S. Sensitivities and uncertainties of modeled ground temperatures in mountain environments. *Geosci. Model Dev.* **6**, 1319–1336 (2013).
38. Draebing, D., Krautblatter, M. & Dikau, R. Interaction of thermal and mechanical processes in steep permafrost rock walls: a conceptual approach. *Geomorphology* **226**, 226–235 (2014).
39. Draebing, D., Haberkorn, A., Krautblatter, M., Kenner, R. & Phillips, M. Thermal and mechanical responses resulting from spatial and temporal snow cover variability in permafrost rock slopes, Steintaelli, Swiss Alps: thermal and mechanical responses to snow in permafrost rock slopes. *Permafrost Periglacial Processes* **28**, 140–157 (2017).
40. Zhang, T. Influence of the seasonal snow cover on the ground thermal regime: an overview. *Rev. Geophys.* **43**, RG4002 (2005).
41. Gruber, S. & Haeberli, W. Permafrost in steep bedrock slopes and its temperature-related destabilization following climate change. *J. Geophys. Res. Earth Surf.* **112**, F02S18 (2007).
42. Hoelzle, M. et al. Long-term energy balance measurements at three different mountain permafrost sites in the Swiss Alps. *Earth Syst. Sci. Data* **14**, 1531–1547 (2022).
43. McColl, S. T. & Draebing, D. in *Geomorphology of Proglacial Systems: Landform and Sediment Dynamics in Recently Deglaciated Alpine Landscapes* (eds Heckmann, T. & Morche, D.) 119–141 (Springer International Publishing, 2019); [https://doi.org/10.1007/978-3-319-94184-4\\_8](https://doi.org/10.1007/978-3-319-94184-4_8)
44. Hales, T. C. & Roering, J. J. Climatic controls on frost cracking and implications for the evolution of bedrock landscapes. *J. Geophys. Res. Earth Surf.* **112**, F02033 (2007).
45. Draebing, D. & Krautblatter, M. The efficacy of frost weathering processes in alpine rockwalls. *Geophys. Res. Lett.* **46**, 6516–6524 (2019).
46. Allen, S. & Huggel, C. Extremely warm temperatures as a potential cause of recent high mountain rockfall. *Glob. Planet. Change* **107**, 59–69 (2013).
47. Delonca, A., Gunzburger, Y. & Verdel, T. Statistical correlation between meteorological and rockfall databases. *Nat. Hazards Earth Syst. Sci.* **14**, 1953–1964 (2014).
48. Strunden, J., Ehlers, T. A., Brehm, D. & Nettesheim, M. Spatial and temporal variations in rockfall determined from TLS measurements in a deglaciated valley, Switzerland. *J. Geophys. Res. Earth Surf.* **120**, 1251–1273 (2015).
49. Corominas, J., Matas, G. & Ruiz-Carulla, R. Quantitative analysis of risk from fragmental rockfalls. *Landslides* **16**, 5–21 (2019).
50. IPCC *Global Warming of 1.5 °C* (eds Masson-Delmotte, V. et al.) (WMO, 2018).

**Publisher's note** Springer Nature remains neutral with regard to jurisdictional claims in published maps and institutional affiliations.

**Open Access** This article is licensed under a Creative Commons Attribution 4.0 International License, which permits use, sharing, adaptation, distribution and reproduction in any medium or format, as long as you give appropriate credit to the original author(s) and the source, provide a link to the Creative Commons licence, and indicate if changes were made. The images or other third party material in this article are included in the article's Creative Commons licence, unless indicated otherwise in a credit line to the material. If material is not included in the article's Creative Commons licence and your intended use is not permitted by statutory regulation or exceeds the permitted use, you will need to obtain permission directly from the copyright holder. To view a copy of this licence, visit <http://creativecommons.org/licenses/by/4.0/>.

© The Author(s) 2024

## Methods

### Dendrogeomorphic sampling of a rockfall slope

Rockfall is the predominant gravitational process at Täschgüfer and has formed several talus slopes with widespread evidence of recent rockfall activity. In the forest, reaching elevations of up to 2,150 m asl at the study site, virtually every tree shows clear evidence of past rockfall impact on the stem surface, predominantly in the form of injuries or broken crowns. To gather a representative dataset of past rockfall activity, we simulated preferential trajectories of rockfall activity on the slope using the three-dimensional, process based RockyFor3D model<sup>51</sup>. On the basis of model results, we defined a 177-m-wide transect at the upper forest fringe where trees intercept rockfall originating from the outcrops upslope and sampled a total of 375 *Larix decidua* trees with 896 increment cores/cross sections during two field campaigns. A first campaign was realized in 2011 during which 252 trees were sampled; a second campaign followed in 2021 (123 trees) to update the reconstruction to the present day. The selection of trees was based on the idea to cover virtually all trajectories while avoiding as much as possible sampling several trees in the direct fall line, as shading effects will lead to an underestimation of activity<sup>27</sup>. Likewise, we made an effort to avoid the sampling of trees that could have been impacted by the same rockfall. In the context of this study, and in view of the nature of and the conditions at the study site, we assume that each scar or growth disturbance (GD) represents an individual rockfall knowing that in exceptional cases, a falling rock can damage more than one tree and that rockfall events may consist of more than just a single rock.

Injuries represent the most accurate and reliable evidence of past rockfall in tree-ring records<sup>52–54</sup>, we therefore searched for fresh and overgrown wounds on the stem surface. The position of each sampled tree was recorded with a <1-m precision global positioning system (GPS) device and located in a geographical information system as geo-objects. The annual rings of trees that survived rockfall impacts were counted inwards from the bark, known from the date of collection, and cross dated using standard dendrochronological procedures<sup>55</sup>. In addition to injuries, dendrogeomorphic indicators of past rockfall also included strong tangential rows of traumatic resin ducts (TRDs). The latter form around an injury within days after mechanical wounding<sup>52,53</sup>. Their use has been proven valuable for the detection and dating of completely overgrown injuries<sup>22</sup>, and even if sampling is done at considerable vertical (>1 m) and/or radial distances from the injury<sup>52,56</sup>. In this paper, and for the analysis of changes in rockfall seasonality, we analyse separately (1) injuries and (2) the combination of injuries and TRDs—which we refer to as GDs—separately. The reason for this distinction is that TRDs can potentially form in later portions of a growth ring (next paragraph provides insights on the seasonality of rockfall) if increment cores are sampled far away from the wound and thus potentially induce a bias<sup>52,53,56,57</sup>. As a result of the comparably small tree diameters involved in this study, this effect can be considered negligible.

### Seasonality of rockfall

In a next step, we used the intra-ring position of all injuries and strong TRDs leaving clear evidence of past rockfall damage in the tree-ring record (ref. 22 provides a rating of GDs) to date past rockfall activity with sub-seasonal precision<sup>52,53,57–59</sup>. We distinguish six sub-annual positions of GDs within individual tree rings (Extended Data Fig. 1): those formed at the precise limit between two rings are attributed to dormancy (D), that is, the time window after the formation of the previous and the onset of subsequent ring formation. Those located in the thin-walled, clearer early wood portion of a ring are attributed to early (EE), middle (ME) and late (LE) early wood, whereas a GD found in the latewood was attributed to either the early (EL) or late (LL) latewood of a given ring. Data exist on the onset and cessation of tree growth in the study region<sup>26</sup>, and the formation of different portions of growth rings can thus be defined as follows: D starts on 1 October 1 and ends on 15 May; EE is defined as 16 May–7 June, ME as 8 June–30 June and LE

as 1 July–15 July. The EL is assumed to be formed between 16 July and 15 August and the LL between 16 August and 30 September. A total of 408 injuries and strong TRDs (1920–2020; out of 1,357 GDs used for the rockfall reconstruction) can be attributed clearly to one of the six sub-seasonal periods defined above.

Because event dates can only be attributed to a certain segment of a tree ring (that is, D, EE, ME, LE, EL and LL), we employed a Monte Carlo simulation to transform sub-seasonal resolution to event dates. For each rockfall dated with injuries ( $n = 83$ ) or GDs ( $n = 408$ ), a day of rockfall occurrence (doy) was defined randomly 1,000 times with a Monte Carlo approach across the range defined for the different sub-segments of a tree ring. For each of the 1,000 iterations, a local polynomial regression was fitted to the doym time series for (1) all injuries and (2) GDs in the period 1920–2020. In addition, we also calculated changes in rockfall seasonality for sub-periods defined as 1920–1969, 1970–2020 and 2010–2020 to detect trends in seasonality. In the next step, we used the same 1,000 iterations to derive quantile-based regressions and the Theil–Sen estimator and to quantify temporal shifts in rockfall occurrence over the past 100 years.

Quantile-based regressions are commonly used to estimate the trend of the median in data for which the conditions of linear regression are not met. The approach was proposed as a way to discover more useful predictive relationships between variables in cases where only a weak relationship exists between the means of variables or where interactions between different factors are complex. The Theil–Sen estimator was used as an additional metric to fit a line to sample points by using the median of the slopes of all lines through pairs of points. As the Theil–Sen estimator is less affected by outliers, it can sometimes be more accurate than other tests.

### Tree-ring-based reconstruction of rockfall activity

When reconstructing rockfall in forests, one needs to consider the area that is covered by trees in a given year, as a changing forest cover and increasingly larger tree diameters (DBH) will influence the likelihood that a rockfall will hit or miss a tree on its trajectory<sup>60</sup>. The probability for a tree to be impacted by a rockfall will thereby depend on the nature of the forest (that is, stand density, tree location, tree diameter, spatial structure of the forest) and the nature of rockfall (mostly block dimensions). To address this challenge, the conditional impact probability approach (CIP; Extended Data Fig. 2) has been employed widely in dendrogeomorphic reconstructions of rockfall activity<sup>27,28,61,62</sup>. It is based on the idea that each tree is surrounded by a ‘circle of impact’ (that is, covering a range of the slope that determines the probability of a tree being impacted).

A falling rock will impact a tree if its trajectory is closer to the stem than half of the rock’s diameter ( $\emptyset$ ). This ‘circle of impact’ can thus be expressed as a circular area around each tree, with its diameter being defined by the tree’s DBH and the mean diameter of falling rocks ( $\emptyset = 0.58$  m in our case). As the DBH of a tree changes over time, we calculate the sum of diameters present in any given year covered by the reconstruction using averaged increment rates of each single tree by dividing individual tree DBH by their age<sup>27,63</sup>. The sum of impact circles of all trees represents the total length of impact circles ( $L_{IC}$ ) or the range that is covered by trees<sup>28</sup>. We present this information in Extended Data Fig. 3 by visually demonstrating the variations in the percentage of the slope covered by trees. These variations are attributed to (1) alterations in the sampled depth and tree diameter over time and (2) the fact that two distinct sampling campaigns were conducted to compile the dataset utilized in this study. Accordingly, with a given mean rock diameter, tree position and the DBH measured for all trees (Supplementary Fig. 4 provides an overview), the CIP can be calculated for a given surface as:

$$CIP = L_{IC}/L_{plot} \quad (1)$$

where  $L_{plot}$  is the width of the plot across the slope in the fall line (that is, 177 m in our case).

The CIP can thereby be used as an estimate of the number of missed (that is, not recorded) rockfalls in a given year—especially at the beginning and the end of the time series—but also quantify the potential overestimation of activity. An overestimation can occur in cases where  $L_{IC}$  exceeds  $L_{plot}$  due to the sampling of more than one tree on a given trajectory. The CIP is therefore also a means to assess the quality and reliability of the reconstruction over time<sup>27,62</sup>.

Extended Data Fig. 3 illustrates the number of trees available for any given year of the reconstruction (Extended Data Fig. 3b) and their cumulated diameter at breast height (Extended Data Fig. 3a). When the cumulated DBH is combined with the circle of impact as defined by the rock diameter, we obtain the percentage of the slope that is covered in every single year of the reconstruction (Extended Data Fig. 3b) and therefore allows the transformation of raw into range corrected rockfall impacts (Extended Data Fig. 3c).

### Climate–rockfall correlations

Reconstructed rockfall activity was correlated against the gridded (1 × 1 km) temperature and precipitation fields for Switzerland extending back to 1763 CE (ref. 64). We selected the grid point centred over the study site and retrieved data for the period 1920–2020. For both datasets, z-scores were preferred over absolute values as they (1) allow calculation of probabilities of a score occurring within a normal distribution and (2) enable comparison between two scores that are from different normal distributions. As such, z-scores represent the number of standard deviations a given data point (here a year) lies above or below the mean of the rockfall activity (expressed as RCI) or air temperature. Mean and standard deviations of the RCI and air temperatures were computed over the full period of the reconstruction (1920–2020). By way of example, a z-score of +1 indicates a value that is one standard deviation from the mean.

Correlations between reconstructed rockfall and mean air temperatures and precipitation totals were computed for (1) seasonal records of mean air temperatures and precipitation totals in a first step. In a second step, to detect possible changes over time, we (2) employed daily climate records averaged over 30- to 504-day time windows starting on 15 May of the year preceding ring formation ( $y - 1$ ) and ending on 30 September of the year in which rockfall was reconstructed ( $y$ ), using the R package *dendroTools*<sup>65</sup>. This second step was realized to identify those time windows (in terms of seasonality and length) that best correlate with rockfall activity and to attempt understanding of drivers underlying slope instability as a result of permafrost degradation.

To test robustness of relations between rockfall activity and climatic parameters, we split the period into two segments of similar length (that is 1920–1969, 1970–2020). Correlations were also computed between rockfall activity and permafrost borehole temperatures at 0.6 m depth at Corvatsch (Swiss Alps, 46° 25' N, 9° 49' E, 2,670 m asl; ref. 42). Permafrost time series are much shorter than meteorological records and cover only the period 2001–2020 (Supplementary Fig. 2).

### Data availability

Daily high-resolution temperature and precipitation fields for Switzerland from 1763 to 2020 are publicly available at <https://doi.org/10.1594/PANGAEA.950236>. Borehole data were retrieved from PERMOS (<http://newshinypermos.geo.uzh.ch/app/DataBrowser/>). All raw data created in this paper are available at <https://doi.org/10.5281/zenodo.10142460>.

### Code availability

All analyses and figure preparation are performed in R programming language. The source codes to reproduce our analysis are available at <https://doi.org/10.5281/zenodo.10142460>. The seasonal trend analysis code is inspired by work published by Heiser et al. (ref. 66).

## References

- Dorren, L. K. A. *Rockyfor3D (v 5.0) Revealed—Transparent Description of the Complete 3D Rockfall Model* (EcorisQ, 2012).
- Schneuwly, D. M., Stoffel, M., Dorren, L. K. A. & Berger, F. Three-dimensional analysis of the anatomical growth response of European conifers to mechanical disturbance. *Tree Physiol.* **29**, 1247–1257 (2009).
- Schneuwly, D. M., Stoffel, M. & Bollschweiler, M. Formation and spread of callus tissue and tangential rows of resin ducts in *Larix decidua* and *Picea abies* following rockfall impacts. *Tree Physiol.* **29**, 281–289 (2008).
- Stoffel, M., Butler, D. R. & Corona, C. Mass movements and tree rings: a guide to dendrogeomorphic field sampling and dating. *Geomorphology* **200**, 106–120 (2013).
- Bräker, O. U. Measuring and data processing in tree-ring research—a methodological introduction. *Dendrochronologia* **20**, 203–216 (2002).
- Bollschweiler, M., Stoffel, M., Schneuwly, D. M. & Bourqui, K. Traumatic resin ducts in *Larix decidua* stems impacted by debris flows. *Tree Physiol.* **28**, 255–263 (2008).
- Stoffel, M. & Hitz, O. M. Rockfall and snow avalanche impacts leave different anatomical signatures in tree rings of juvenile *Larix decidua*. *Tree Physiol.* **28**, 1713–1720 (2008).
- Schneuwly-Bollschweiler, M. & Stoffel, M. Hydrometeorological triggers of periglacial debris flows in the Zermatt valley (Switzerland) since 1864. *J. Geophys. Res. Earth Surf.* **117**, F02033 (2012).
- Stoffel, M., Ballesteros Cánovas, J. A., Luckman, B. H., Casteller, A. & Villalba, R. Tree-ring correlations suggest links between moderate earthquakes and distant rockfalls in the Patagonian Cordillera. *Sci. Rep.* **9**, 12112 (2019).
- Perret, S., Stoffel, M. & Kienholz, H. Spatial and temporal rockfall activity in a forest stand in the Swiss Prealps—a dendrogeomorphological case study. *Geomorphology* **74**, 219–231 (2006).
- Moya, J., Corominas, J., Pérez Arcas, J. & Baeza, C. Tree-ring based assessment of rockfall frequency on talus slopes at Solà d'Andorra, Eastern Pyrenees. *Geomorphology* **118**, 393–408 (2010).
- Favillier, A. et al. Dendrogeomorphic assessment of rockfall recurrence intervals at Saint Paul de Vances, Western French Alps. *Géomorphol. Relief Processus Environ.* <https://doi.org/10.4000/geomorphologie.11681> (2017).
- Morel, P., Trappmann, D., Corona, C. & Stoffel, M. Defining sample size and sampling strategy for dendrogeomorphic rockfall reconstructions. *Geomorphology* **236**, 79–89 (2015).
- Imfeld, N., Pfister, L., Brugnara, Y. & Brönnimann, S. A 258-year-long data set of temperature and precipitation fields for Switzerland since 1763. *Clim Past* **19**, 703–729 (2023).
- Jevšenak, J. & Levanič, T. *dendroTools*: R package for studying linear and nonlinear responses between tree-rings and daily environmental data. *Dendrochronologia* **48**, 32–39 (2018).
- Heiser, M., Schlögl, M., Scheidl, C. & Fuchs, S. Comment on 'Hydrometeorological triggers of periglacial debris flows in the Zermatt Valley (Switzerland) since 1864' by Michelle Schneuwly-Bollschweiler and Markus Stoffel. *J. Geophys. Res. Earth Surf.* **127**, e2021JF006562 (2022).

## Acknowledgements

We are grateful to S. Belin-Gorsic, L. Blaser, M. Farvacque and M. Karrer for their help during fieldwork and sample analysis. We acknowledge K. Tscherrig for multiple first-hand information on and eyewitness reports of recent rockfalls.



### Author contributions

M.S. and C.C. designed the study with input from all co-authors. All authors participated in fieldwork and analyses of tree-ring data. C.C. and M.S. performed analyses and wrote a first draft of the paper; all co-authors provided comments and revisions.

### Funding

Open access funding provided by University of Geneva

### Competing interests

The authors declare no competing interests.

### Additional information

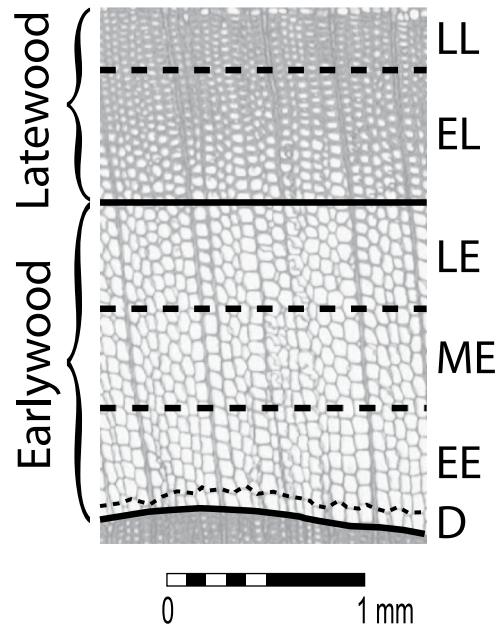
**Extended data** is available for this paper at <https://doi.org/10.1038/s41561-024-01390-9>.

**Supplementary information** The online version contains supplementary material available at <https://doi.org/10.1038/s41561-024-01390-9>.

**Correspondence and requests for materials** should be addressed to Markus Stoffel.

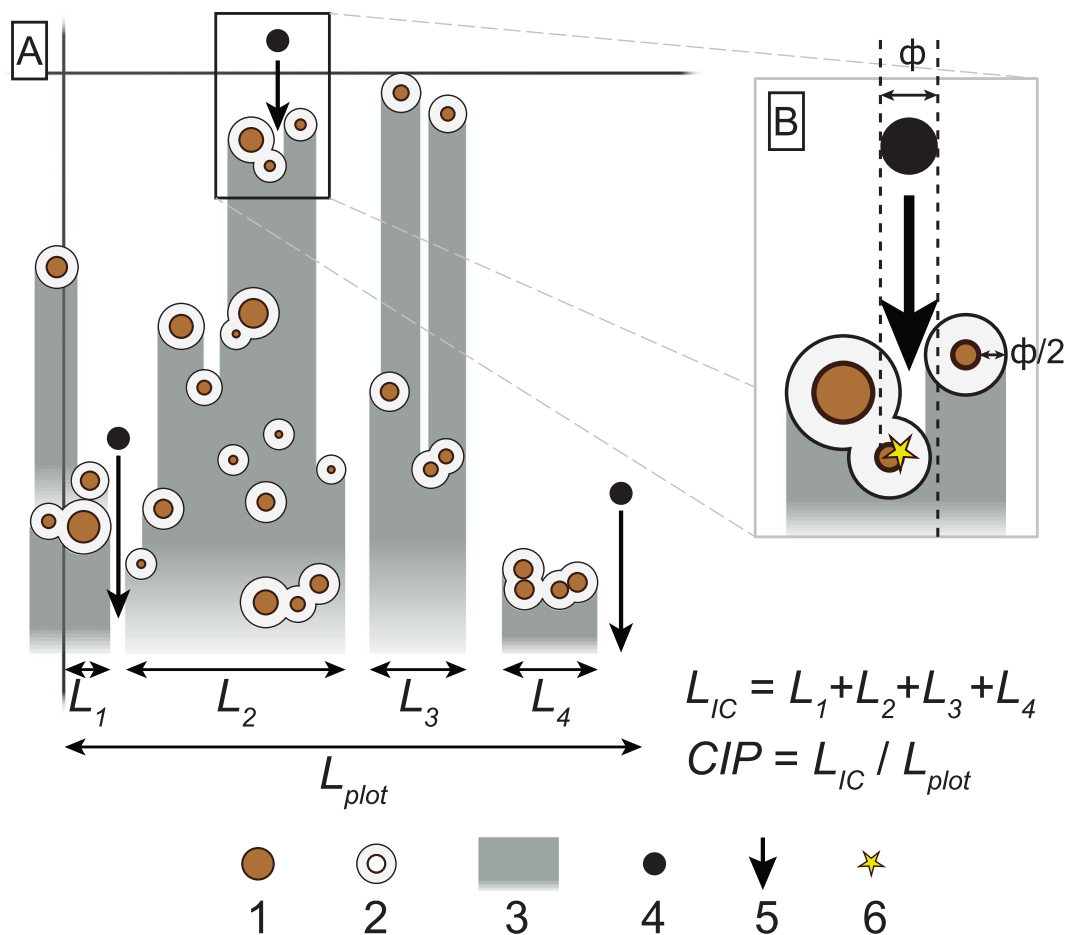
**Peer review information** *Nature Geoscience* thanks Else van den Besselaar, Brian Luckman and the other, anonymous, reviewer(s) for their contribution to the peer review of this work. Primary Handling Editor: Tom Richardson, in collaboration with the *Nature Geoscience* team.

**Reprints and permissions information** is available at [www.nature.com/reprints](http://www.nature.com/reprints).



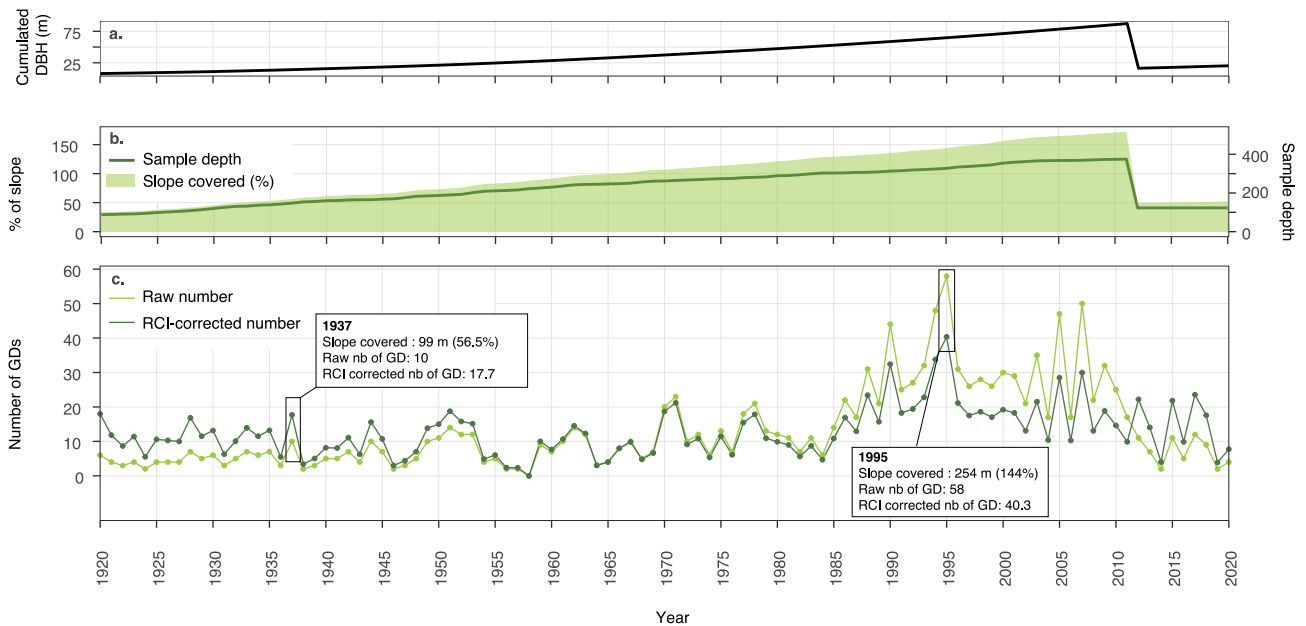
**Extended Data Fig. 1 | Subdivision of annual increment of conifer trees into several sub-segments.** In this study, we subdivided individual rings into thin-walled earlywood (E) and thick-walled latewood (L) cell layers. At the end of the growing season, cell formation ceases and dormancy (D) starts. Any damage occurring during dormancy will occur at the contact between the previous and

the new ring. E is subdivided into early (EE), middle (ME) and late (LE) earlywood, L into early (EL) and late (LL) latewood. This subdivision was applied to locate scars and tangential rows of traumatic resin ducts within a tree ring and hence to date past rockfall with sub-seasonal precision.



**Extended Data Fig. 2 | Definition and calculation of conditional probability of a rock impacting a tree on a slope.** (a) The Conditional Impact Probability (CIP)<sup>27,61</sup> considers the distribution of trees within a given plot. (b). Computation of impact circles. 1. Tree stem; 2. Circle of impact; 3. Projection of

the circles of impacts to the bottom boundary of the cell analyzed; 4. Rock of a given diameter; 5. Trajectory of the falling rock; 6. Rockfall impact.  $L_1$ ,  $L_2$ ,  $L_3$  and  $L_4$  are the widths of the projection of the circles of impact at the bottom of the cell. LIC is the width of the analyzed cell. Adapted from Ref. 62.



**Extended Data Fig. 3 | Evolution over time of tree diameters, sample depth and length equivalent to the slope width sampled. (a)** Changes in the cumulated sum of all tree diameter (in m), **(b)** number of trees in the chronology (sample depth) and the length equivalent to the slope width (177 m) that was sampled (in %) for every year between 1920 and 2020. **(c)** Raw numbers of

Year

rockfall impacts (injuries or GD) are corrected following the conditional impact probability (CIP) approach, resulting in the inclusion of more events in the chronology for years in which only part of the slope width is covered and in a reduction of events whenever the sum of diameters exceeds the slope width (177 m). The years 1937 and 1995 are selected here to illustrate the conversion.